Seasonality of coastal upwelling off central and northern California: New insights, including temporal and spatial variability

M. García-Reyes[1] and J. L. Largier[1]

Received 26 September 2011; revised 23 January 2012; accepted 26 January 2012; published 17 March 2012.

[1] The coastal ocean environment off California is largely determined by wind-driven coastal upwelling, with an ecosystem that is tightly coupled to seasonality in this upwelling. Three decades of data measured over the California shelf at NOAA buoys are used to describe the seasonal variability of the winds that force upwelling and the response of the coastal ocean in terms of sea temperature. Moreover, seasonal patterns in surface chlorophyll and alongshore currents are determined from one decade of data. In addition to clear seasonality, all these data exhibit distinct spatial and non-seasonal temporal variability in upwelling. Based on alongshore wind stress characteristics in central and north California, three seasons are defined: Upwelling Season (April-June) with strong upwelling-favorable winds and large standard deviation due to frequent reversals; Relaxation Season (July-September) with weak equatorward winds and low variability; and Storm Season (December-February) characterized by weak mean wind stress but large variability. The remaining months are transitional, falling into one or other season in different years. In addition to large-scale latitudinal differences in wind stress, spatial differences are associated with coastal topography - specifically the acceleration of wind downstream of capes. Latitudinal differences in sea surface temperature depend on wind stress, both local and large-scale, but also on surface heating and offshore influences. Intra-annual and inter-annual anomalies in wind and sea surface temperature are associated with variability in coastal winds, large-scale winds, and offshore basin-scale ocean conditions. Satellite chlorophyll concentration shows an optimal window relation with upwelling forcing, allowing maximum concentrations during moderate winds and minimal during poor or strong winds.

Citation: García-Reyes, M., and J. L. Largier (2012), Seasonality of coastal upwelling off central and northern California: New insights, including temporal and spatial variability, *J. Geophys. Res.*, *117*, C03028, doi:10.1029/2011JC007629.

1. Introduction

[2] The coastal ocean environment off California is largely determined by wind-driven coastal upwelling, with an ecosystem that is tightly coupled to seasonality of upwelling. This process, observed also in other eastern boundary current systems, is driven by equatorward alongshore wind stress that through forcing divergence in surface Ekman transport brings cold and nutrient-rich deep waters to the euphotic zone, resulting in high levels of primary production and a highly productive ecosystem. This wind stress is the surface expression of geostrophic winds driven by a cross-shore pressure gradient that, in the Northeast Pacific, develops during the spring/summer between the North Pacific High (NPH) and the Continental Thermal Low (CTL) pressure systems [*Huyer*, 1983; *Murphree et al.*, 2003]. At the coast, the wind is constrained and modified by the Marine Atmospheric Boundary Layer (MABL) and the topography [*Halliwell and Allen*, 1987; *Beardsley et al.*, 1987; *Winant et al.*, 1988; *Koračin et al.*, 2004; *Ström and Tjernström*, 2004], resulting in strong and highly polarized alongshore winds [*Bakun and Nelson*, 1991; *Dorman and Winant*, 1995].

[3] The seasonality of coastal upwelling was recognized long ago in the four eastern boundary upwelling systems [see *Chavez and Messié*, 2009, and references therein]. However, many descriptions are based on short-term or coarse-scale data or they focus only on the upwelling season [*Huyer*, 1983; *Strub et al.*, 1987; *Bakun and Nelson*, 1991; *Nykjær and Van Camp*, 1994]. In California a full-year description of coastal upwelling based on 10 years of buoy data was given by *Dorman and Winant* [1995], but due to the marked differences in the nature of the winter and summer winds, seasonality was described by the average characteristics of these two seasons and it has continuously been described in this form [*Halliwell and Allen*, 1987; *Murphree et al.*, 2003]. While useful in describing annual values, this bimodal seasonality does not capture aspects that are relevant to the ecosystem - for example, the transition time from

[1]Bodega Marine Laboratory, University of California, Davis, Bodega Bay, California, USA.

0148-0227/12/2011JC007629

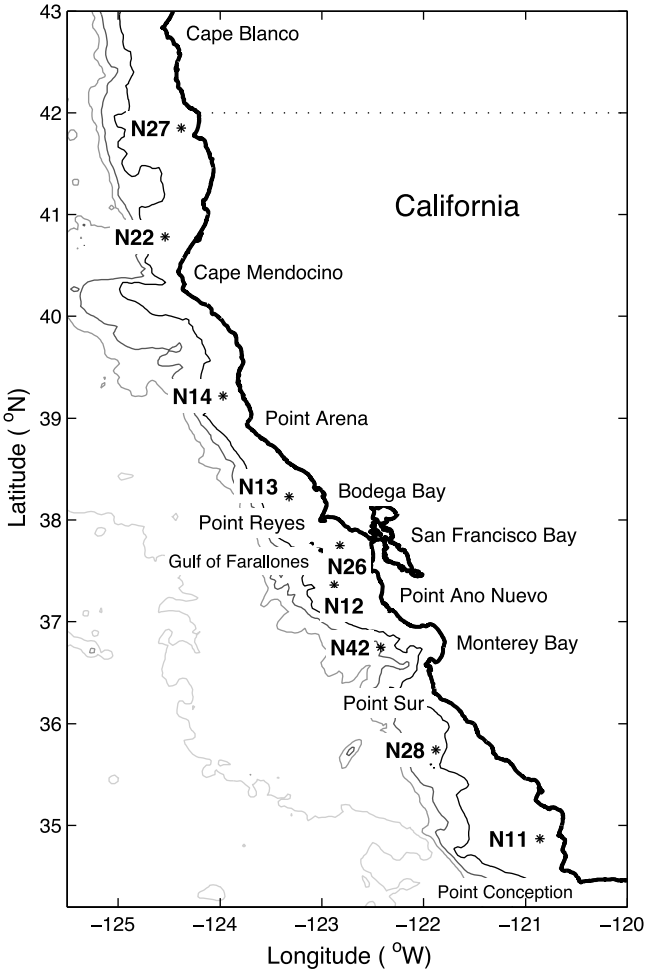

Figure 1. NDBC buoy locations over the Californian continental shelf.

winter to upwelling conditions [*Strub et al.*, 1987; *Lentz*, 1987; *Lynn et al.*, 2003], the delay of which could cause failures in biological productivity [*Sydeman et al.*, 2006; *Barth et al.*, 2007], or the differences in upwelling during the year, that leads to the bloom of different species of phytoplankton depending on the time of year [*Estrada and Blasco*, 1979; *Kudela et al.*, 2005].

[4] Many studies, in particular in ecology [*Kahru et al.*, 2009; *Thomas et al.*, 2009], use the Coastal Upwelling Index (UI) instead of wind. The UI quantifies the Ekman transport caused by the stress exerted by geostrophic winds that are in turn calculated from measurements of large-scale atmospheric pressure gradients across the coast [*Bakun*, 1973]. The UI has been useful in tracking the variability of upwelling and ocean conditions in the California Current System (CCS) on inter-annual scales [*Schwing et al.*, 2006; *Bograd et al.*, 2009; *Black et al.*, 2011]. However, for more local analyses, it misrepresents the wind-forcing (and thus upwelling intensity) since it has a coarse spatial resolution (3° Latitude) and does not account for effects of topography, atmosphere and ocean conditions at the local scale [*Halliwell and Allen*, 1987; *Dorman and Winant*, 1995; *Winant et al.*, 1988; *Burk and Thompson*, 1995; *Pickett and Schwing*, 2006]. Differences between the UI and in-situ measured winds may be significant in terms of influences on local biological productivity [*Vander Woude et al.*, 2006].

[5] In California long time series of measured data are available now from satellites, HF-radar and buoys. These allow us to describe the seasonality of coastal upwelling and coastal conditions robustly, on both local and regional scales, increasing our understanding of local-scale interactions of processes within the coupled ocean/land/atmosphere system. They provide us with a more accurate quantification of the deviations from the seasonal cycle, and a better understanding of the nature of such anomalies and their effects on the coastal conditions and the ecosystem.

[6] In this study we analyze 29 years of measured data from the Californian coast to describe the seasonality of coastal upwelling forcing and physical and biological response over the continental shelf. We compare the local winds with the UI to identify key differences through the year, and to explore the role of local features in modifying geostrophic winds near the coast. We also describe seasonal anomalies in winds and temperatures at intra-annual and inter-annual timescales and compare them to large-scale climate oscillations to investigate the influence of large-scale dynamics on coastal conditions. Finally we use satellite-based chlorophyll concentration to observe the effect of coastal upwelling on primary productivity.

2. Data

[7] Time series of hourly wind velocity and sea surface temperature (SST) from 1982 to 2010 are obtained from 9 coastal buoys maintained by the National Data Buoy Center (NDBC, http://www.ndbc.noaa.gov/) of the National Oceanic and Atmospheric Administration (NOAA). The locations of the buoys are shown in Figure 1 and details are given in Table 1. SST data are also obtained from an offshore buoy (N59: 38.0°N, 130.0°W). Wind stress is calculated following *Large and Pond* [1981]. The alongshore component of the wind stress is calculated in the direction of the principal axis of the wind at each buoy, since coastal winds are in the alongshore direction (Table 1). Since only this component is analyzed, we referred to it here simply as τ (without subscript). Daily averages of the parameters are calculated and gaps in the data, including the initial gap where some buoys were deployed after 1982, are filled using data from the nearest buoys since wind and SST are highly correlated between neighboring buoys (details given by

Table 1. NDBC Buoy Information[a]

Buoy	Lat (°N)	Lon (°W)	I. Year	C. Orien.	P. Axis
N27	41.85	124.38	1983	345	338
N22	40.78	124.54	1982	357	351
N14	39.22	123.97	1981	333	328
N13	38.23	123.32	1981	310	312
N26	37.75	122.82	1982	310	320
N12	37.36	122.88	1980	333	327
N42	36.75	122.42	1986	330	326
N28	35.74	121.88	1983	325	320
N11	34.87	120.86	1980	327	320

[a]Buoy is the buoy label, Lat (°N) is latitude (degrees north), Lon (°W) is longitude (degrees west), I. Year is the initial year of data, C. Orien. is the coastal orientation angle from *Dorman and Winant* [1995] (clockwise degrees from true north), and P. Axis is the principal axis of the wind at that point.

García-Reyes and Largier [2010]). The daily alongshore wind stress component measured at the buoys is referred to here as τ_b.

[8] Daily means of coastal UI for the US West coast are calculated by the Pacific Fisheries Environmental Laboratory of NOAA (available from http://www.pfeg.noaa.gov), with a resolution of 3° Latitude. To compare with τ_b, UI values were linearly interpolated for each buoy location, and then the alongshore wind stress obtained by reversing the calculation of Ekman transport (see *Bakun* [1973] for details). The resulting geostrophic calculated wind stress is referred to here as τ_g.

[9] The time series of daily τ_b, τ_g, and SST were filtered with a low-pass filter (10-day cut-off period), thus removing variability at wind-event timescales, i.e., synoptic variability. These filtered daily data are used in the harmonic analysis and in the calculation of anomalies and standard deviations, but the results are averaged monthly. Ranked correlations and further filtering are performed with the monthly data.

[10] In order to study the nature of τ and SST anomalies, they are compared with time series of climate indices. The Multivariate El Niño-Southern Oscillation (ENSO) Index (MEI, available from http://www.esrl.noaa.gov/psd/people/klaus.wolter/MEI/table.html) is a comprehensive index of tropical conditions that relate to the El Niño events. This index includes atmospheric (sea level pressure, surface wind, surface air temperature, and total cloudiness fraction of the sky), and oceanic (SST) parameters over the tropical Pacific. The Pacific Decadal Oscillation index (PDO, available at http://jisao.washington.edu/pdo/PDO.latest) measures a multidecadal variability in SST over the North Pacific with a contrasting signature along US West coast [*Mantua and Hare*, 2002]. Finally, the North Pacific Gyre Oscillation (NPGO, available at http://www.o3d.org/npgo/data/NPGO.txt) index tracks the low-frequency variability of sea surface height over the North Pacific, and has been correlated to upwelling variability along the coast of North America [*Di Lorenzo et al.*, 2008, 2009].

[11] Another parameter to characterize upwelling is alongshore surface current, which is available from HF-radar measurements for different time periods along the coast of California (see data details and Figure 5 in the work of *Bjorkstedt et al.* [2010]) [see also *Kaplan et al.*, 2005; *Kim et al.*, 2011]. Hourly data on flow past Point Reyes (38°N) are available since 2001 and this location downstream of buoy N13 is chosen to study the seasonality of the equatorward surface flow over the shelf. Data were obtained from the Bodega Ocean Observing Node at BML/UCDavis (http://www.bml.ucdavis.edu/boon/hf_radar.html). Spatial averages are obtained for two regions west of Point Reyes (one inshore of 123°W, same longitude as N13, and the other offshore of 123°W). The north-south component of the flow is chosen since the principal component is along this axis.

[12] As a proxy for biological productivity over the shelf, monthly chlorophyll concentration (Chl) data from the SeaWiFS satellite are used, available from 1998 to 2006 with a resolution of 9 × 9 km^2 (http://oceancolor.gsfc.nasa.gov/). A line along the shelf that passes through the buoys was chosen to match the physical data from the buoys. It is worth noting that both chlorophyll and SST at the buoys reflect an accumulation of processes upstream of the buoy (i.e., to the north and on shore during upwelling), whereas wind is a local measurement and one can expect some mismatch in linking these indices of upwelling forcing and response. Along the chosen line, boxes of 3 × 3 grid points (27 × 27 km^2) are averaged to produce a data set without gaps that can be compared with data from the buoys and still conserve spatial resolution and full coverage along the coast.

3. Seasonal Cycle

3.1. Buoy Wind Stress (τ_b)

[13] The seasonal cycle of τ_b can be described by the sum of annual and semiannual harmonics (Figure 2 and Table 2), which explains over 25% of variance (except for buoys N11 and N12) at timescales longer than 10 days ($p < 0.01$). This seasonality is the dominant signal and the other 70% of the variance is distributed uniformly across intra-annual and inter-annual frequencies. The inclusion of higher harmonics does not significantly increase the amount of variance explained, indicating that the recurrent cycle is no more complex than that described by a sum of annual and semiannual harmonics. Spring and summer are characterized by strong upwelling events lasting few to several days [*Beardsley et al.*, 1987; *Dorman and Winant*, 1995] that, on average, affect the climatology but they are not individually captured by the harmonics.

[14] Strongest upwelling (negative τ_b) occurs around May, earlier and stronger in the south with two spatial maxima: one at N13 (Bodega Bay) and another at N28 (south of Point Sur). In July wind stress weakens rapidly, and it remains weak until October. South of buoy N14, τ_b remains upwelling favorable all year, while to the north τ_b reverses during the winter. The seasonal characteristics of τ_b divide the study region into two areas, north and south of Cape Mendocino: northern California (buoys N22 and N27) and central California (buoys N14 to N11). Similar differences in the seasonal wind have been observed along the CCS and other upwelling systems [*Strub et al.*, 1987; *Dorman and Winant*, 1995; *Bakun and Nelson*, 1991; *Chavez and Messié*, 2009].

[15] Seasonal τ does not fully represent the wind characteristics since wind has large high-frequency variability, as seen in the monthly distributions of daily τ in Figure 3a. The strongest northerly winds occur from April to June, as the climatology indicates, but there are also many days of weak winds and several days of southerly winds (wind reversals). From July to September, the wind is weaker but reversals are rare. In October the northerly winds strengthen again, and one sees the start of the southerly wind events that occur during the passage of the cold fronts in winter months. From November to March, winds are strong and may be equatorward or poleward. As averages values do not indicate the variability in wind, winds are best described by a combination of mean and standard deviation (Figure 4).

[16] The upwelling season is often considered to be from May to August, and the seasonality is described in a bimodal way, contrasting average conditions during the summer with the winter [*Halliwell and Allen*, 1987; *Murphree et al.*, 2003; *Dorman and Winant*, 1995]. However, when monthly mean and standard deviation of τ_b are considered (Figure 4), three clear clusters emerge. (i)

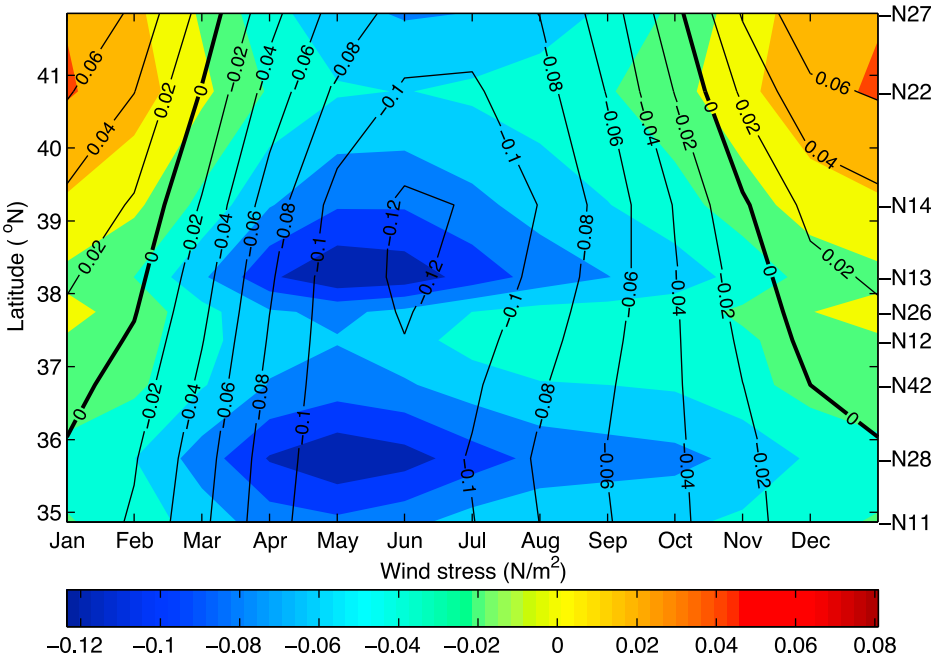

Figure 2. Climatology of alongshore wind stress (τ) from annual and semiannual harmonics. Color: τ_b. Lines: τ_g.

Dec-Jan-Feb - weak mean τ_b with large standard deviation due to the occurrence of strong southerly wind events that contrast with a background of northerly winds; (ii) Apr-May-Jun - strong negative (upwelling favorable) winds and large standard deviation, due to frequent wind relaxations and reversals; and (iii) Jul-Aug-Sep - weakly equatorward winds, few reversals and low standard deviation. The other months (March, October and November) are considered transition months as they fall into one or other season in different years, depending on the timing of the transitions between seasons. Therefore, three seasons are defined to best represent the annual cycle of τ_b along central and northern California. Following the nomenclature used by *Largier et al.* [1993], but updating the durations, they are defined as: "Storm Season" or winter (December-February), "Upwelling Season" (April-June), and "Relaxation Season" (July-September).

3.2. Geostrophic Wind Stress (τ_g)

[17] The seasonality of τ_g is largely captured by the annual harmonic, which explains over 50% of the variance at timescales longer than 10 days ($p < 0.01$), but for consistency both the annual and semiannual harmonics were calculated (Figure 2 and Table 3). The τ_g is minimum (i.e., most negative) during the upwelling season, although the peak occurs later than for τ_b in central California: about two weeks later in daily data (Table 3), and a month later in monthly data (Figure 2). The seasonal magnitude of τ_g is larger than that of τ_b, with exception of N13 and N28. A single upwelling maximum of τ_g is observed around buoys N13 and N14, with the alongshore pattern of τ_g more uniform than the τ_b pattern due to the UI spatial scale. During the relaxation season, τ_g weakens more uniformly and more slowly than τ_b (Figure 3b), and the correlation between τ_g and τ_b is at its minimum during this period. Also, from March to August, fewer days of calm wind are observed in the τ_g record than in the τ_b record. In winter τ_g reverses north of 36°N whereas τ_b reverses only north of 39°N.

[18] To observe this difference in more detail, we plot daily τ_b against τ_g for all buoys. Figure 5 shows this plot for buoy N13, where the strongest upwelling along the California coast occur (see also section 3.3). Three key differences are noted: (i) τ_b is generally weaker than τ_g at most locations, although this is different for N13 and N28 where τ_b is comparable with τ_g for strong upwelling-favorable winds. (ii) Poleward winds (positive τ) are stronger for τ_g than for τ_b, specifically during the storm season. (iii) Observation of zero τ_b is common, while τ_g are concurrently non-zero -many of these data are from the relaxation season as τ_b decreases to zero quicker than τ_g. While it is clear that τ_g and τ_b exhibit a non-linear seasonal relationship, it is interesting to note that the direction of winds is consistent most of the time (bottom right and top left quadrants in Figure 5 are mostly unoccupied).

Table 2. Parameters of Annual and Semiannual Harmonics of τ_b[a]

		Annual Harmonic			Semiannual Harmonic		
Buoy	Mean	Amplitude	Phase	EV	Amplitude	Phase	EV
N27	−0.0177	0.0499	187	32	0.0073	113	1
N22	−0.0059	0.0403	186	27	0.0095	111	1
N14	−0.0338	0.0447	176	31	0.0121	122	2
N13	−0.0609	0.0499	169	33	0.0168	125	4
N26	−0.0300	0.0272	164	24	0.0144	116	7
N12	−0.0301	0.0192	160	12	0.0147	118	7
N42	−0.0384	0.0252	168	20	0.0127	119	5
N28	−0.0715	0.0359	166	23	0.0164	124	5
N11	−0.0458	0.0212	158	19	0.0129	119	7

[a]Annual mean in N/m^2, amplitude in N/m^2, phase (in this case the strongest wind (negative)) in days, and EV (explained variance) in %.

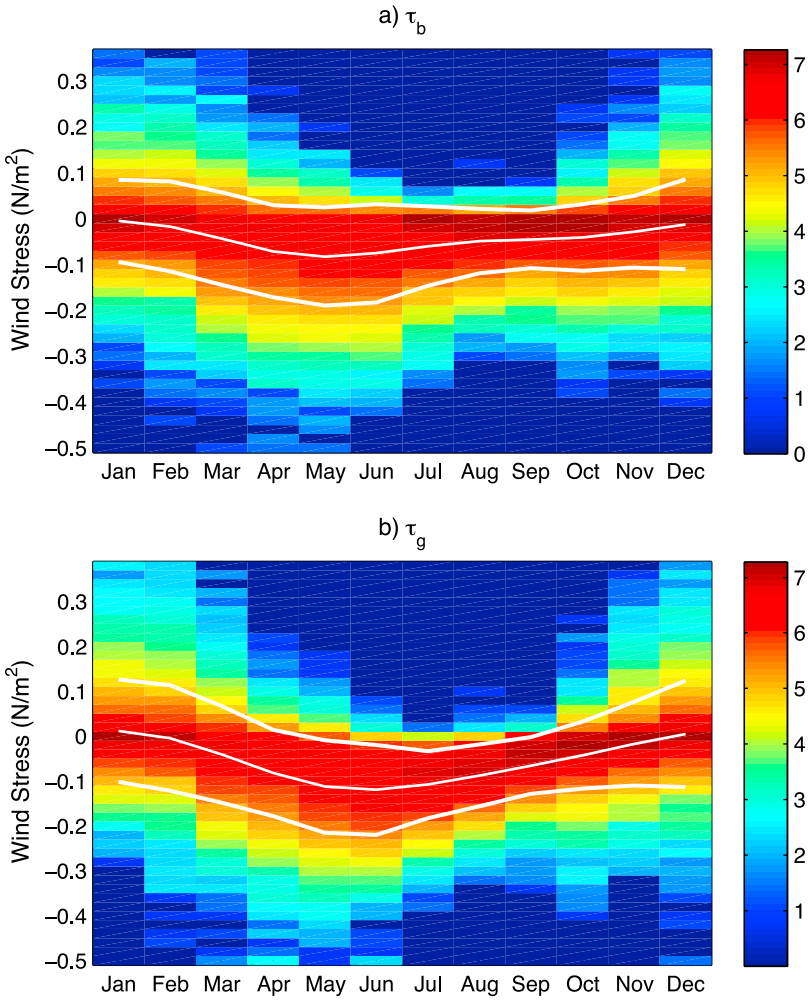

Figure 3. Monthly distribution of daily τ for central California (buoys N14 to N11). Color indicates the frequency of occurrence of τ of a given strength, and white lines indicate the monthly climatology of τ plus/minus the monthly standard deviation. (a) τ_b and (b) τ_g.

[19] A plot of monthly means versus standard deviation of τ_g (not shown) is similar to that of τ_b (Figure 4) - strong wind and high standard deviation during the upwelling season, weak winds and variability in the relaxation season, and low mean wind but large standard deviation during the storm season. However τ_g values are less clustered since it changes more gradually through the year than τ_b. Since the focus of this study is on conditions over the shelf, we use the definition of seasons given by winds measured over the shelf (i.e., τ_b).

3.3. Sea Surface Temperature

[20] The climatology of SST is also described by annual and semiannual harmonics, which account for 30 to 50% of the variance at timescales longer than 10 days ($p < 0.01$) for central California, but less for northern buoys where warming during the relaxation season is weak (Figure 6 and Table 4). Minimum SST over the shelf occurs during the upwelling season, whereas offshore at buoy N59 the minimum temperature occurs in March, at the end of the storm season (Figure 7). After the upwelling season, a rapid increase in SST leads to a maximum over the shelf in September, late in the relaxation season, and about a month after the offshore SST maximum. A north-south gradient in SST is observed, with a local alongshore minimum around Bodega Bay (N13), consistent with the maximum in upwelling-favorable τ_b. Since this location shows the strongest upwelling forcing and response in California, we focus some of the analysis here. The SST minimum extends north to N14, consistent with the minimum in τ_g (i.e., maximum in upwelling-favorable winds). At N28 however, no minimum in SST is observed, nor a local minimum in τ_g.

[21] It is worth noting that coastal SST is cooler than offshore SST year-round (Figure 7). *Dever and Lentz* [1994], by considering coastal heat balances, showed that the seasonality of SST in an upwelling system is due to three primary influences: (i) offshore SST, which varies seasonally due to surface heating and seasonality in the California Current, (ii) upwelling of cold waters due to the wind, which also varies seasonally, and (iii) local surface warming of coastal waters. The first and third terms are seasonal warming effects that are represented by the seasonal signal in offshore SST, while the seasonal variability in the upwelling effect is associated with the seasonality of local τ (Figure 7). A multivariate linear regression of coastal SST with offshore SST (indexed by the temperature at N59, but corrected by

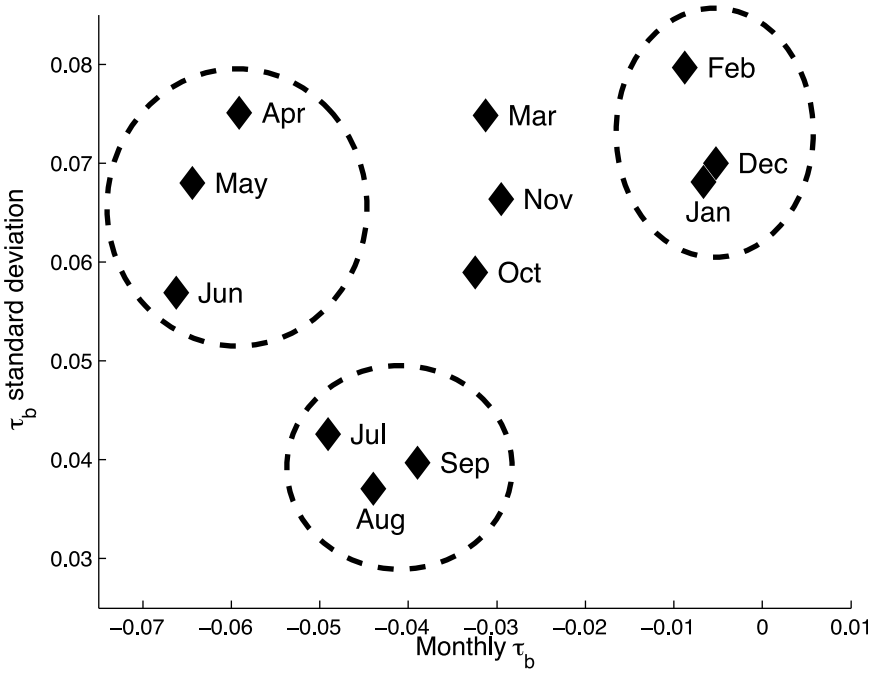

Figure 4. Monthly τ_b versus τ_b standard deviation. Median values from all buoys and all years.

the latitude of each buoy) and τ_b, shows that offshore SST is always dominant. However, τ_b has a cooling effect on coastal SST year-round: strongest during the upwelling season (particularly at N13), weaker during the relaxation season, and minimum during the storm season.

3.4. Other Parameters

3.4.1. Surface Flow

[22] A decade of HF-radar data over the central California shelf shows that surface flow is primarily wind-driven, as previously described by *Strub et al.* [1987], *Winant et al.* [1987], and *Steger et al.* [2000], although there are also influences from offshore circulation in the California Current [*Largier et al.*, 1993; *Lynn et al.*, 2003; *Kaplan et al.*, 2007]. Throughout the study region, surface flow is southward during the upwelling season, weak during the relaxation season and weakly northward in the storm season, with eddies developing downstream of major headlands [*Bjorkstedt et al.*, 2010; *Halle and Largier*, 2011; C. M. Halle et al., manuscript in preparation, 2012].

[23] The climatology from annual and semiannual harmonics of the northward current past Point Reyes explains 51 and 45% ($p < 0.01$) of the monthly variability (Figure 8) in nearshore and offshore locations respectively. This is similar to the seasonality of τ_b at N13, particularly offshore, but with peak currents preceding peak τ_b by about a month (Figure 8). Equatorward flow shows a rapid increase in March to a maximum during the upwelling season, with flow slower nearshore than farther offshore. In June, a reduction in flow at offshore locations is observed, despite the fact that τ is still strong, consistent with previous reports [*Largier et al.*, 1993, Figure 18]. During the relaxation season weak flow is observed, and near-zero monthly mean flows during the storm season. A comparison between surface flow and τ_g seasonality (not shown) indicates a larger lag in the timing of seasonal peaks in currents and τ_g.

3.4.2. Chlorophyll Concentration

[24] The climatology of Chl from annual and semiannual harmonics, explains about 36% of the variance ($p < 0.01$) of the 9-year record of monthly satellite ocean color data (Figure 9). Although important latitudinal variations are observed, there is seasonal coherence across the study region with Chl increasing at the beginning of the upwelling season (Mar-Apr) to reach a maximum in June. Chl decreases during the relaxation season, and it is minimum during the storm season. The seasonal increment of Chl with upwelling, due to the input of nutrients to the euphotic zone, is also seen in the Canary Current Upwelling System, but not in others upwelling systems [*Chavez and Messié*, 2009].

[25] Chl values are highly variable year to year due to strong event-scale variability, however a scatterplot of monthly means of Chl against τ_b (Figure 10) shows that high Chl values are only observed during months with moderate

Table 3. Parameters of the Annual and Semiannual Harmonics of the τ_g Interpolated at the Location of Each Buoy[a]

		Annual Harmonic			Semiannual Harmonic		
Buoy	Mean	Amplitude	Phase	EV	Amplitude	Phase	EV
N27	−0.0133	0.0878	188	51	0.0080	94	0
N22	−0.0276	0.0839	187	51	0.0069	106	0
N14	−0.0485	0.0784	185	48	0.0081	125	1
N13	−0.0532	0.0711	182	50	0.0094	127	1
N26	−0.0542	0.0671	180	51	0.0100	127	1
N12	−0.0550	0.0639	179	52	0.0105	127	1
N42	−0.0564	0.0591	175	51	0.0112	128	2
N28	−0.0587	0.0534	171	51	0.0119	128	3
N11	−0.0611	0.0534	170	58	0.0109	128	2

[a]Annual mean in N/m^2, amplitude in N/m^2, phase (in this case the strongest wind (negative)) in days, and EV (explained variance) in %.

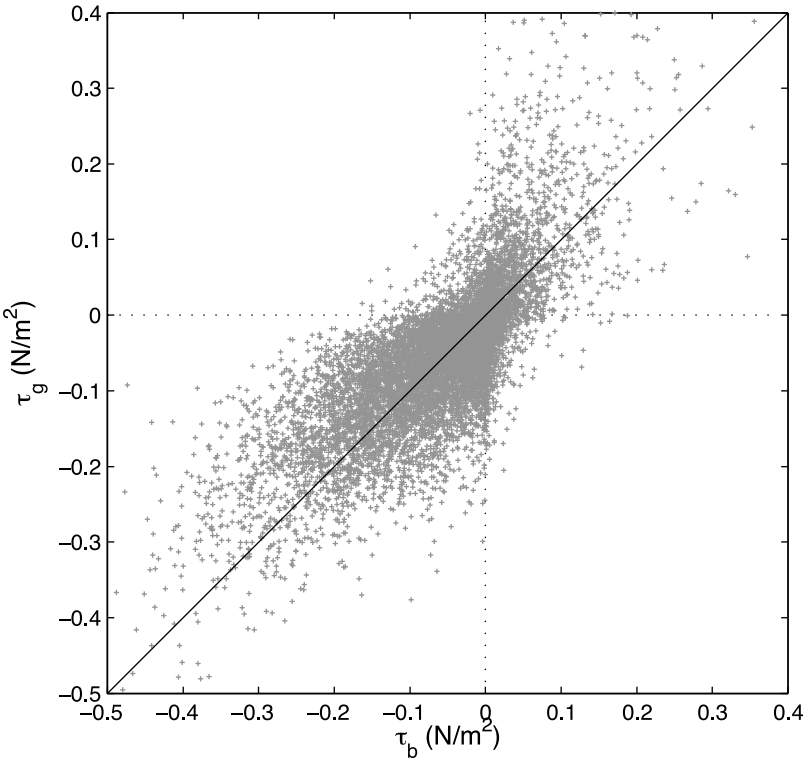

Figure 5. Daily τ_b versus τ_g at buoy N13. Black line shows equal values.

upwelling-favorable winds (upwelling and relaxation seasons), but not during months with the strongest winds (and strongest offshore advection). This is in agreement with the mid-range optimum ideas outlined by *Botsford et al.* [2003, 2006] and *Cury and Roy* [1989]. Low-chlorophyll months however, are independent of the magnitude of τ_b and occur throughout the year.

[26] Alongshore, maximum Chl is found in the Gulf of Farallones (37–38°N), where Chl remains high from March through November. A secondary spatial maxima is observed off northern California (between Cape Blanco in Oregon and Cape Mendocino) in Jun-Jul. Just north of Point Reyes, in the vicinity of buoy N13, maximum Chl is observed in October, apparently transported north from the Gulf of Farallones. Another point of interest is around 35°N, where

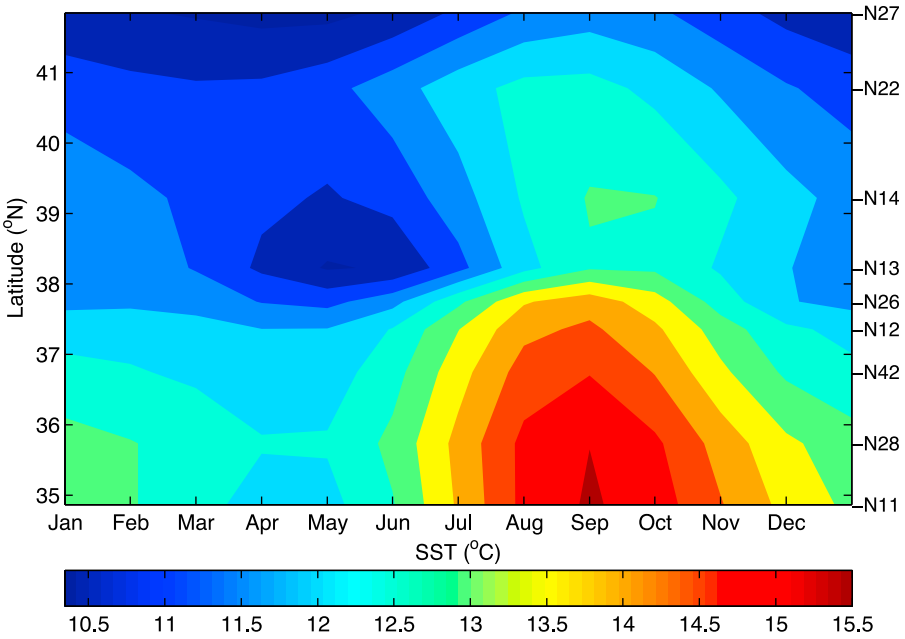

Figure 6. SST climatology from annual and semiannual harmonics (°C).

Table 4. Parameters of SST Annual and Semiannual Harmonics[a]

		Annual Harmonic			Semiannual Harmonic		
Buoy	Mean	Amplitude	Phase	EV	Amplitude	Phase	EV
N27	10.92	0.699	84	16	0.202	158	1
N22	11.76	0.847	66	22	0.138	143	1
N14	11.96	0.985	105	28	0.290	165	2
N13	11.76	1.070	119	30	0.480	162	6
N26	12.49	1.290	79	38	0.596	158	8
N12	13.00	1.231	76	43	0.460	156	6
N42	13.29	1.320	78	44	0.450	157	5
N28	13.76	1.400	85	45	0.425	156	4
N11	13.79	1.562	92	47	0.406	153	3

[a]Annual mean in °C, amplitude in °C, phase (i.e., the coldest water) in days, and explained variance (EV) in %.

high Chl levels could be associated with transport from the Southern California Bight.

4. Anomalies

[27] The seasonal cycle represents a recurrent pattern that may be considered "typical", but deviations from this pattern occur frequently and they are likely to have an impact on the ecosystem if notably large or persistent. Previous studies have found a trend of increasing upwelling winds in some upwelling areas, including central California [*Bakun*, 1990; *Bograd et al.*, 2002; *Mendelssohn and Schwing*, 2002; *García-Reyes and Largier*, 2010], however this trend is accompanied by large inter-annual and decadal variability. In the CCS, this variability is associated with fluctuations in the Pacific Ocean climate - mainly ENSO and PDO [*Lluch-Cota et al.*, 2001; *Schwing et al.*, 2002; *Mendelssohn, et al.*, 2003; *Legaard and Thomas*, 2006; *Chhak and Di Lorenzo*, 2007; *Thomas et al.*, 2009]. However, most studies in California focus on changes at the CCS spatial scale and not at local coastal scales. Here we calculate monthly anomalies as deviations from the local harmonic seasonal cycle to identify major anomalous events or recurrent types of anomaly, at local and regional scales.

4.1. Wind Stress and SST

[28] The strongest anomalies of τ_b are concurrent along the coast (Figure 11), but they are typically larger at N13 and N28, since the harmonic seasonality does not capture the remarkably strong wind events observed at these locations. Anomalies in τ_g are more coherent in time and space, owing to the coarse resolution of the UI, but anomalies in some years are larger in northern California. Large anomalies in τ_b, τ_g, and SST occur mostly at the same time, but some years anomalies are only visible in one or two of the parameters, and in general, SST anomalies are more persistent (Table 5).

[29] Many anomalies of τ are short-lived (less than a month) which are considered as unusual events, longer and stronger than typical upwelling events, rather than as a true seasonal anomaly that represents season-wide conditions in a specific year. The analysis of this high-frequency variability is beyond the scope of this seasonal analysis. Here we focus on more persistent anomalies, and separate them into intra-annual (3–12 month timescales) and inter-annual scales (longer than a year). The time series of monthly anomalies is bandpass filtered to extract intra-annual frequencies, and low pass filtered to extract inter-annual anomalies (Figure 12).

4.1.1. Intra-annual Anomalies

[30] Intra-annual variance accounts for about 25% of τ_b and 30% of τ_g monthly anomalies, with the strongest variability for τ_b in the vicinity of the Gulf of Farallones and south of 37°N for τ_g. The rest of the variance is divided into inter-annual and high-frequency variability (<3 months). Intra-annual variability of SST accounts for 30% of the monthly anomaly variance, and the correlation between

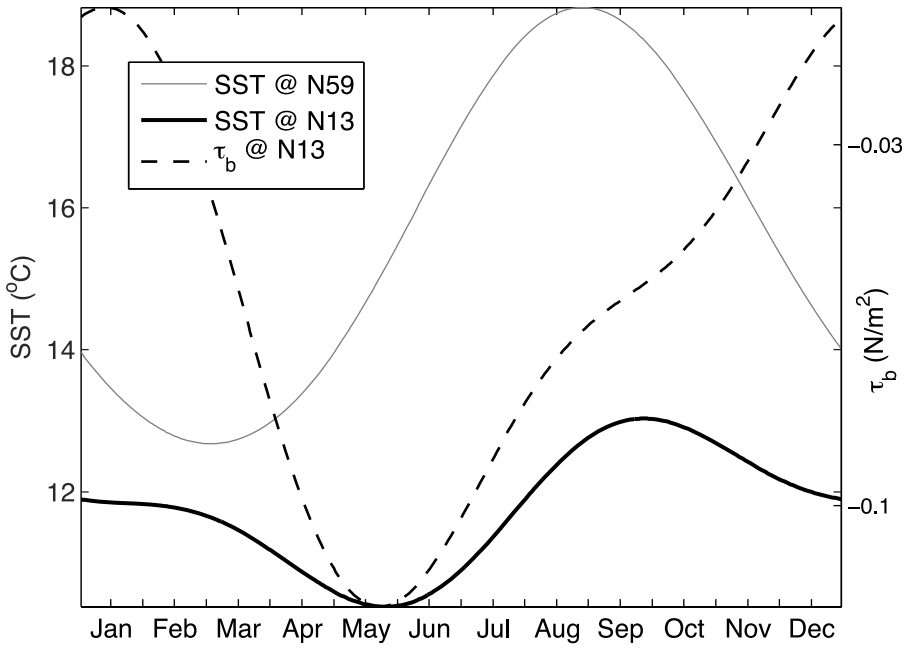

Figure 7. SST climatology for N13. Black solid line: SST data from N13; gray solid line: offshore SST (buoy N59); dashed line: τ_b at N13.

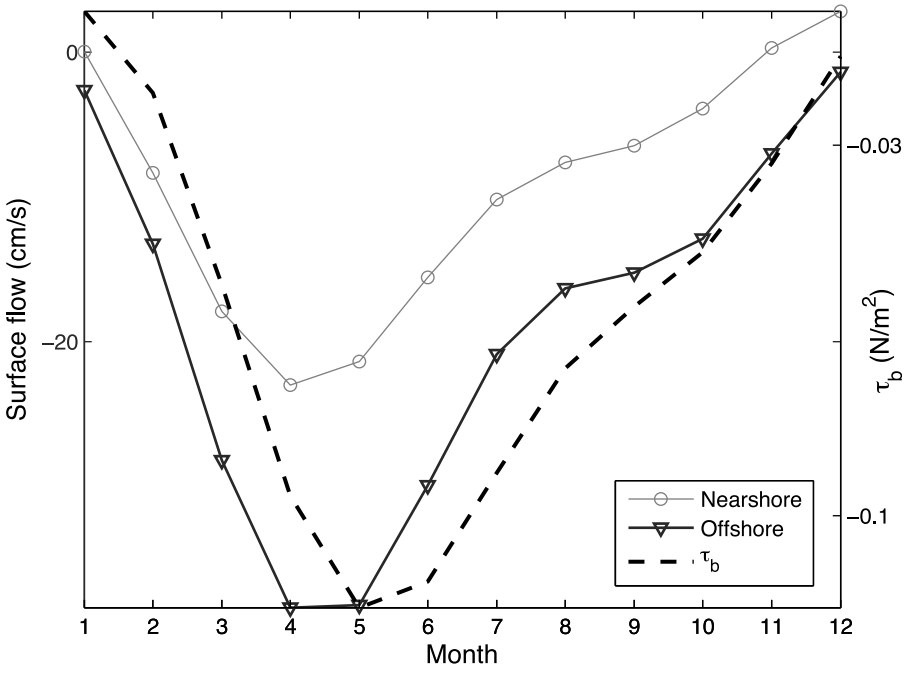

Figure 8. Climatology, from harmonics, of surface flow off Point Reyes and τ_b at buoy N13. Circles: Nearshore flow. Triangles: Offshore flow. Dashed line: τ_b.

intra-annual SST and τ_b and τ_g is, on average, 0.5 - with best correlations for buoys N14 to N12.

[31] Anomalous wind and SST conditions along California can be related to climate forcing, and here we choose climate indices that have been related to changes in upwelling. (i) MEI has being used to explain anomalies in physical and biological parameters off California [*Lluch-Cota et al.*, 2001; *Schwing et al.*, 2002; *Mendelssohn and Schwing*, 2002; *Legaard and Thomas*, 2006; *Thomas et al.*, 2009] and exhibits strong inter-annual variability. (ii-iii) PDO and NPGO have distinctive signatures in wind and SST off the US west coast [*Lluch-Cota et al.*, 2001; *Mantua and Hare*, 2002; *Mendelssohn et al.*, 2003; *Di Lorenzo et al.*, 2008; *Thomas et al.*, 2009] and exhibit both inter-annual and decadal variability.

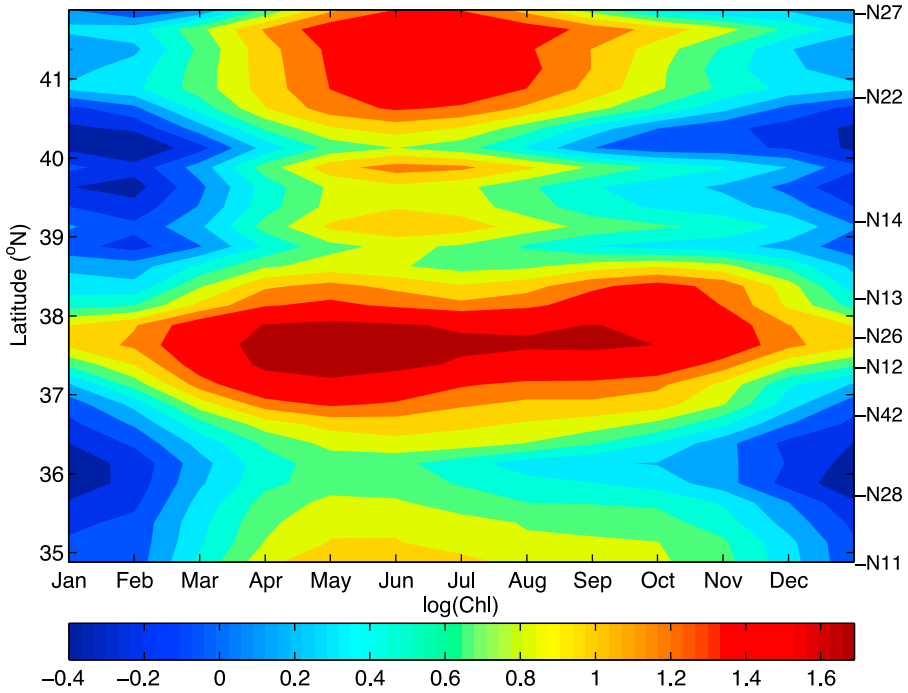

Figure 9. Climatology, from harmonics, of chlorophyll concentration (mg/m^3), in logarithmic scale.

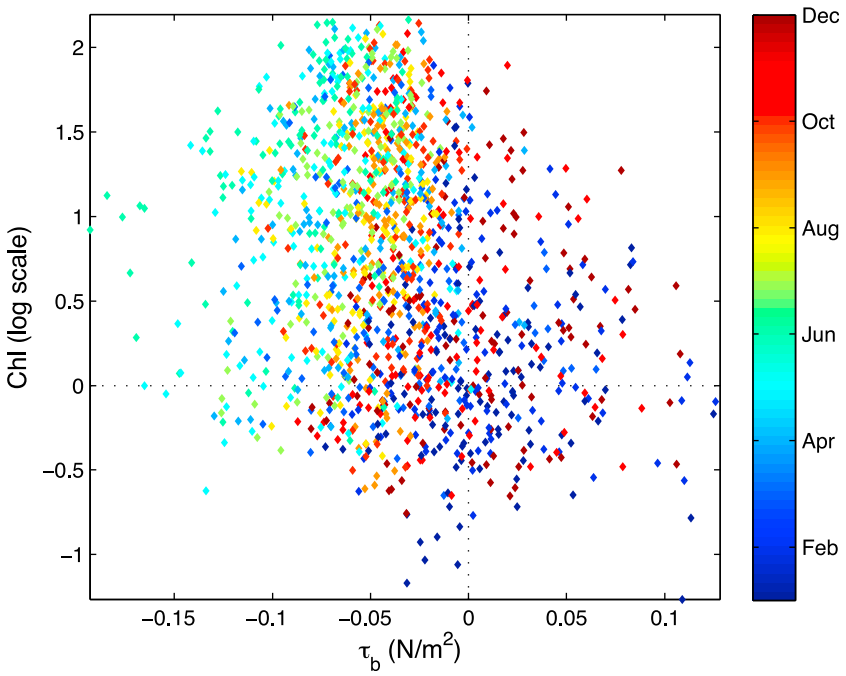

Figure 10. Monthly τ_b versus chlorophyll concentration for all buoys. Chl in logarithmic scale.

[32] Correlations between the climate indices and intra-annual variability in τ and SST were calculated, however only correlations with PDO are significant, although weak (Figure 13). For τ_b, significant correlations occur only for buoys N14 to N27. For τ_g and SST, correlations are best in the north, and decreasing to the south.

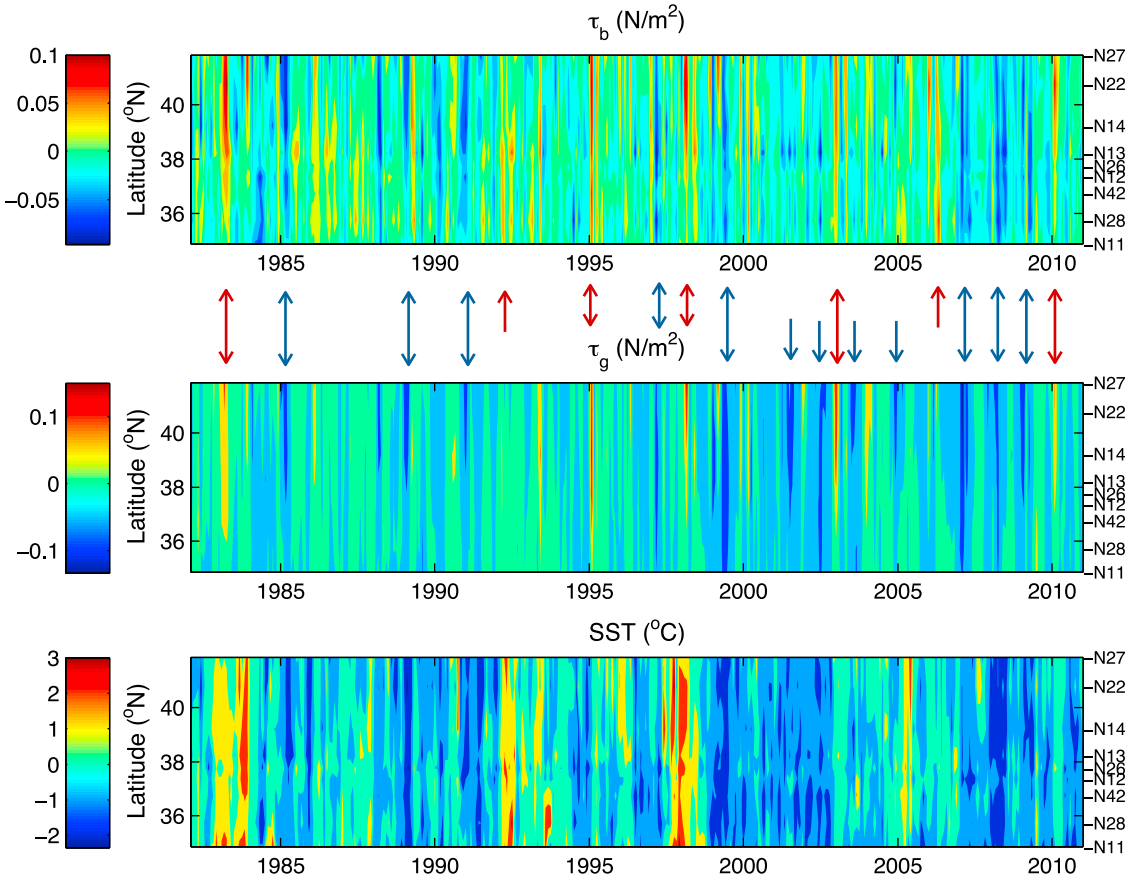

Figure 11. Monthly anomalies of τ_b, τ_g, and SST.

Table 5. Year and Sign of Large Anomalies in τ_b, τ_g, and SST

Year	τ_b	τ_g	SST
1983	+	+	+
1985	–	–	–
1989–1991	–	–	–
1992	+		+
1995	+	+	
1997	–	–	
1998	+	+	+
1999	–	–	–
2000		–	–
2003	+	+	–
2005			+
2006	+		
2007–2009	–	–	–
2010	+	+	

4.1.2. Inter-annual Anomalies

[33] For wind stress, the inter-annual component is less important that the intra-annual, accounting for about 20% of the τ_g and about 13% of the τ_b variance. Inter-annual variability is largest in the Gulf of Farallones vicinity (buoys N26 to N42) and, for τ_b it drops off to the north. Inter-annual variability in SST is important, accounting for 40% of the anomaly signal, with a correlation >0.65 with inter-annual τ_g.

[34] Correlations between the climate indices and the inter-annual component of τ and SST are shown in Figure 14. While τ_b correlates similarly with all climate indices at most central buoys ($r > 0.3$), maximum correlations of ~0.5 are seen with MEI and NPGO at buoys N13, N26 and N11. On the other hand, τ_g correlations show a greater difference between climate indices. Correlation with PDO has a north-south gradient with large values (up to 0.52) for the northern buoys, while correlations with MEI are strongest and >0.4 for the Point Reyes-Point Arena area (buoys N14-N12). NPGO correlations have a north-south gradient too, largest south of Point Reyes (37°N). The inter-annual SST signal exhibits strongest correlations with MEI and PDO ($r \sim 0.6$). However, it is interesting to note that a few SST anomaly events cannot be related to τ anomalies or to climate indices, e.g., low SST and weak negative anomaly for τ in 1985.

4.2. Spring Transition

[35] The beginning of the upwelling season, known as the "spring transition" [*Strub et al.*, 1987; *Lentz*, 1987; *Lynn et al.*, 2003], is marked by an increase in the magnitude and persistence of equatorward τ, and it is an important factor for the ecosystem, as it marks an increased availability of nutrients and thus the start of the season of high primary

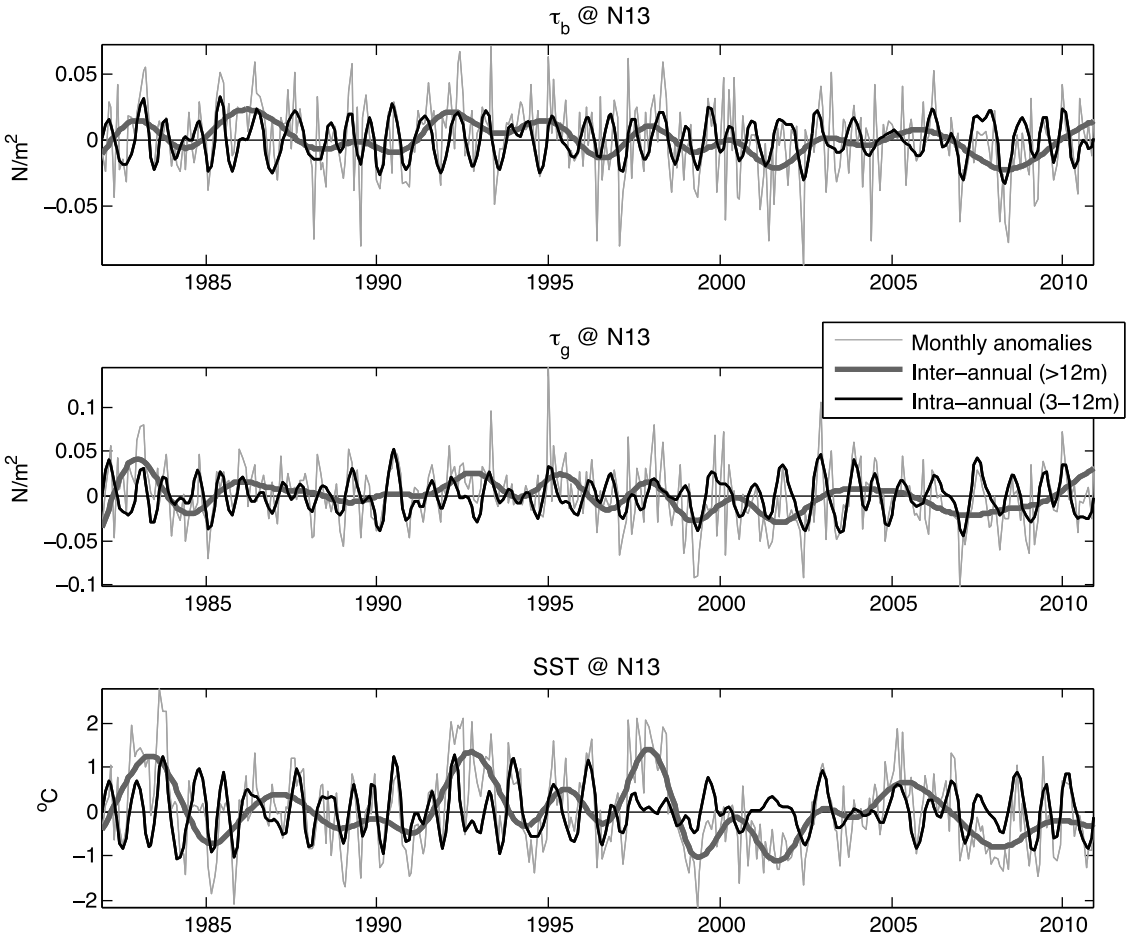

Figure 12. Monthly anomalies of τ_b, τ_g and SST for N13, and time series of inter-annual and intra-annual anomalies.

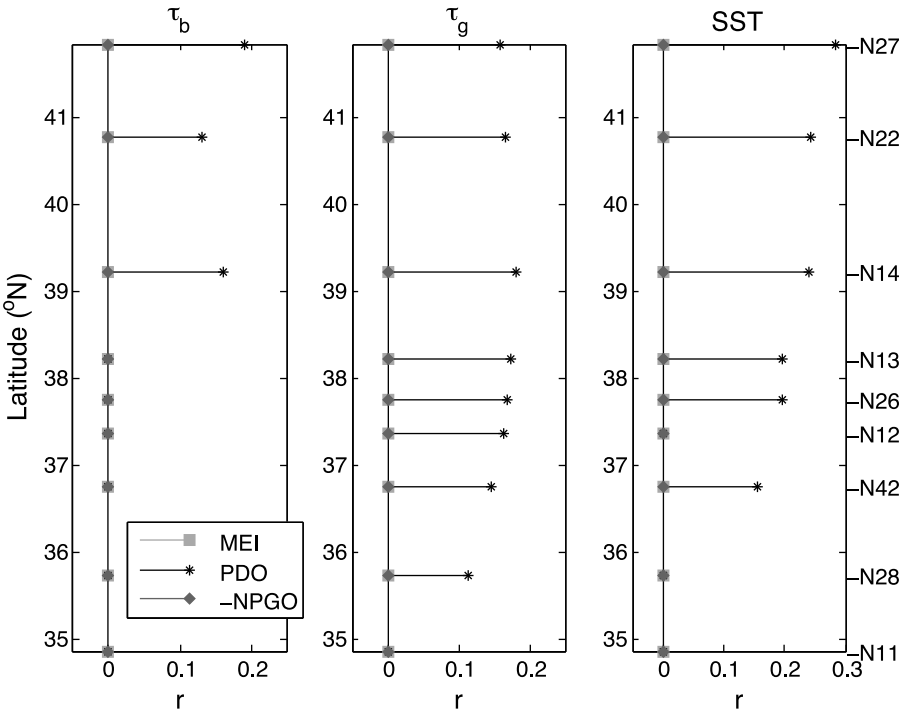

Figure 13. Significant correlations ($p < 0.05$) between climate indices and intra-annual component of τ and SST anomalies.

production [*Lynn et al.*, 2003; *Sydeman et al.*, 2006; *Barth et al.*, 2007]. It is also important as it determines the relative phasing of marine population phenology (e.g., timing of spawning or rearing), plankton dispersal, and environmental conditions [*Largier*, 2003; *Shanks and Roegner*, 2007; *Sydeman and Bograd*, 2009, and references therein]. Defining the spring transition here through an increase in wind stress and an increase in the persistence of upwelling-favorable wind (> 50% of days with wind speeds > 5 *m/s* in the following 30 days), we determine the week of the spring transition each year (see Figure 15 for N13). Clearly, upwelling favorable τ starts earlier in the south than in the

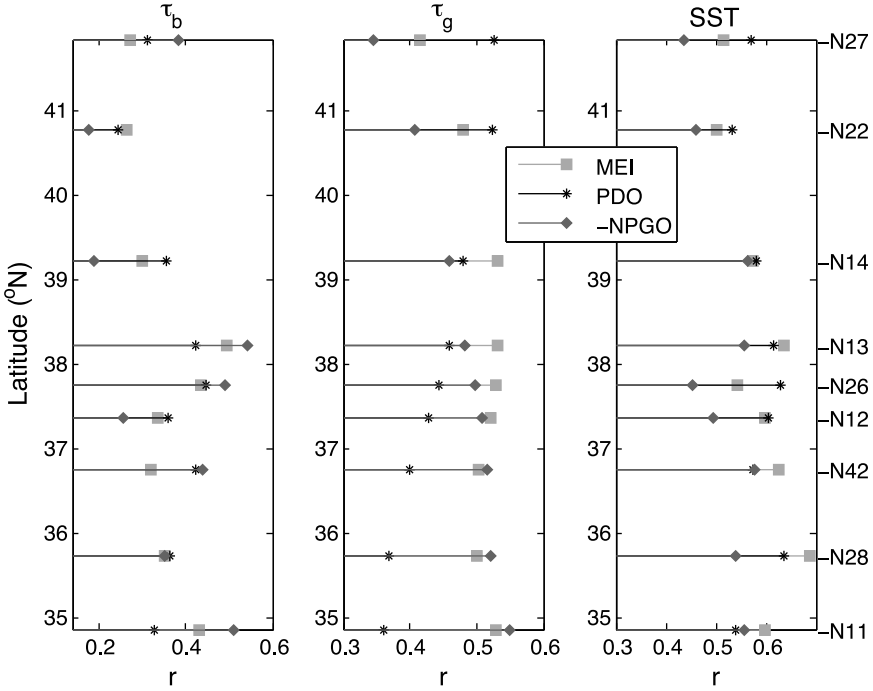

Figure 14. Significant correlations ($p < 0.05$) between climate indices and inter-annual component of τ and SST anomalies.

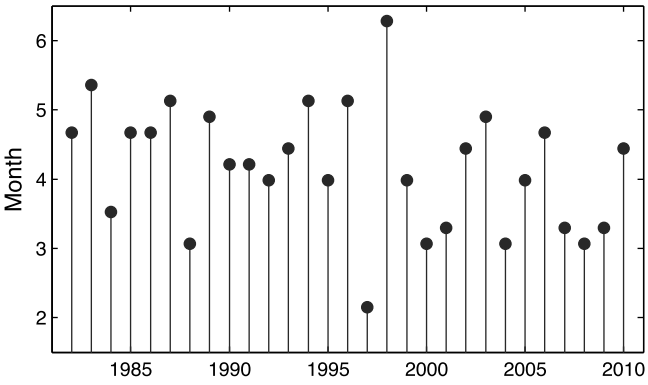

Figure 15. Timing of spring transition for buoy N13.

north (Figure 2), but on average April is the first month dominated by upwelling conditions, and the year to year variability is similar between buoys.

[36] The spring transition is not significantly correlated with the climate indices, but anomalous years can be related to climatic events, particularly with ENSO, i.e. 1998. Further, a trend for earlier spring transition has been observed since the 1980s, as reported by *Bograd et al.* [2002] and *García-Reyes and Largier* [2010]. In years with an earlier spring transition, the upwelling season exhibits stronger mean wind stress and colder SST.

4.3. Anomalies in Other Parameters

[37] Chlorophyll anomalies (not shown) have a similar latitudinal pattern to Chl seasonality, but on average, large anomalies are different between northern and central California. Chl exhibits large negative anomalies in 1998 and 1999, in particular for the Gulf of Farallones and positive anomalies in 2005 and 2006 for all central California. In other years anomalies are small and brief. While negative anomalies of Chl are observed for strong negative τ_g (upwelling favorable winds), chlorophyll anomalies do not have a consistent relationship with τ or SST anomalies.

[38] Alongshore surface flow around Point Reyes varies significantly year to year and anomalies may last several months (not shown). Noticeable anomalies include stronger flow in 2004 and 2007, weaker flow in 2006 and equatorward flow persisting late in 2005. Anomalies in the surface flow off Point Reyes do not show a relationship with τ_b at N13. However, positive anomalies of surface flow correspond with positive anomalies in τ_g, suggesting large-scale influences of the California Current and mesoscale meanders [*Halle and Largier*, 2011].

[39] Anomalies of Chl and surface flow have correlations with the climate indices of $r < 0.3$, some of them not significant, therefore their relationship is not considered further in this analysis. Furthermore, these time series are short, in particular for correlations with ocean related climate indices, for which variability is at longer timescales than the decade-long record of Chl and currents.

5. Discussion

5.1. Seasonal Cycle

[40] Based on the mean and variance of τ_b off California (Figure 4) the annual cycle is divided into three distinctive seasons: Upwelling (April-June), Relaxation (July-September) and Storm (December-February). This new data-based seasonal definition improves on prior analyses that used a single mean value for May to August to characterize upwelling [*Halliwell and Allen*, 1987; *Dorman and Winant*, 1995; *Murphree et al.*, 2003], although other authors have made some distinction in the winds between spring and summer, within the upwelling period [*Huyer*, 1983; *Largier et al.*, 1993; *Bond et al.*, 1996]. This separation is important because it allows us to resolve the different relationships between SST and τ and between τ_b and τ_g for the upwelling and relaxation seasons.

[41] The Upwelling Season is characterized by geostrophic wind blowing from the northwest [*Strub et al.*, 1987; *Murphree et al.*, 2003]. However, it is the combined influence of the topography and the positive ocean-atmosphere feedback from low SST nearshore that polarizes and strengthens the wind in the alongshore direction [*Beardsley et al.*, 1987; *Winant et al.*, 1988; *Dorman and Winant*, 1995; *Burk and Thompson*, 1995; *Koračin et al.*, 2004; *Ström and Tjernström*, 2004]. Hence, this season is marked by strong and persistent equatorward τ, interrupted by distinct "relaxation" events (weak or reversed winds as observed in Figure 3 and described by *Beardsley et al.* [1987] and *Dorman and Winant* [1995]) associated to coastally trapped disturbances [*Nuss et al.*, 2000]. However, these coastal disturbances are not captured by τ_g, resulting in less relaxation days in the τ_g record than for τ_b. The strong upwelling continuously brings cold water to the surface, which results in a SST minimum during this season (Figure 6) and the pumping of nutrients from below the mixed layer into the euphotic zone allowing phytoplankton to grow (Figure 9). Furthermore, weak stratification and the offshore shoaling of isotherms due to positive wind stress curl [*Bakun and Nelson*, 1991; *Murphree et al.*, 2003] facilitate the upwelling of deep water [*Lentz and Chapman*, 2004; *Kudela et al.*, 2005; *Chavez and Messié*, 2009]. The strong upwelling during this season favors fast-growing diatoms [*Estrada and Blasco*, 1979; *Kudela et al.*, 2005; *Wilkerson et al.*, 2006], leading to the high Chl levels observed. Relaxation events, although not captured by the climatology, slow or halt offshore transport and allow productive waters to remain over the shelf where they can fuel zooplankton and in turn support higher trophic levels [*Botsford et al.*, 2003, 2006]. Surface flow is also at its maximum, although mean flow is slower nearshore (Figure 8) due to frequent flow reversals that occur during relaxation events [*Send et al.*, 1987; *Kaplan et al.*, 2005; *Kaplan and Largier*, 2006].

[42] During the Relaxation Season there is a gradual change in τ_g (Figures 2 and 3), in association with gradual changes in large-scale pressure systems. This weakens τ_b and therefore, coastal upwelling, allowing SST to increase and disrupting the positive feedback to the MABL and the local acceleration of winds near the coast [*Winant et al.*, 1988]. Therefore, a local and rapid change in τ_b is observed in July, decreasing upwelling further and leading to the rapid observed increase in SST as well (Figures 2 and 6). In the relaxation season, reversal events are less frequent (Figure 3). While the nature of these events is still not fully understood [*Nuss et al.*, 2000], differences in the frequency of events have been found between spring and summer by

Bond et al. [1996]. This suggests that relaxation events are related to the atmospheric conditions that prevail during the upwelling season but not during the relaxation season. Nutrient flux to the euphotic zone is weaker in this season due to weaker wind-forcing and the shallower origin of upwelled waters due to higher stratification [*Lentz and Chapman*, 2004; *Kudela et al.*, 2005]. However, elevated chlorophyll levels persist in retention zones (Figure 9), mostly from dinoflagellates, which are more motile than diatoms and thrive in stratified conditions as they can move deeper to access nutrients and shallower to access light [*Estrada and Blasco*, 1979; *Kudela et al.*, 2005]. In addition, flow speeds decrease as upwelling winds weaken, allowing phytoplankton blooms to remain longer over the shelf and be advected poleward (Figure 8).

[43] The Storm Season is characterized by strong, highly variable winds, with no preferred direction (Figure 3) [*Halliwell and Allen*, 1987]. The NPH has migrated south and the CTL has dissipated, so that the central and northern California coast is dominated by frequent storms coming from the north [*Halliwell and Allen*, 1987; *Beardsley et al.*, 1987; *Largier et al.*, 1993]. In this season, strong poleward τ_g is observed, but mean τ_b values are near-zero (Figure 5). It is worth noting that the differences between τ_b and τ_g in all seasons could be the result of the UI calculation: (i) from its coarse resolution, which does not reflect the topographical barriers that nearshore wind encounters blowing poleward, and (ii) from the constant drag coefficient value used in the calculation of the wind stress [*Bakun*, 1973] which in reality changes with the wind velocity and atmospheric conditions [*Large and Pond*, 1981]. While upwelling events occur in the storm season (Figure 3), and despite the weak stratification due to low temperatures and wind mixing [*Murphree et al.*, 2003], primary production and chlorophyll levels are low (Figure 9) due to reduced light availability resulting from short days, high turbidity and deep mixing of photosynthesizing phytoplankton - all factors that vary with latitude. However, recent work suggests that conditions in the storm season could have an impact on the timing of upwelling and the ecosystem conditions during the subsequent upwelling season [*Lentz*, 1987; *Schroeder et al.*, 2009; *Black et al.*, 2011]. While the first important upwelling event usually occurs in March [*Lentz*, 1987], as the cross-shore pressure gradient starts forming again, having important consequences for the ecosystem [*Sydeman et al.*, 2006; *Barth et al.*, 2007], the upwelling winds only become persistently strong in April in most years.

5.2. Spatial Patterns

[44] Latitudinal differences in τ are caused by coastal topography. Most notably, the local minimum of τ_b at N13 and N28 are associated with Point Arena and Point Sur, respectively. As the wind diverges when turning around these capes the shallow MABL transitions to supercritical flow (i.e., a "hydraulic drop") with shallower MABL and accelerated wind speed [*Winant et al.*, 1988; *Dorman et al.*, 2000; *Koračin et al.*, 2004; *Rahn et al.*, 2011]. As a result, τ_b can exceed τ_g at buoys N13 and N28 (Figure 5), since the scale at which the τ_g field is calculated does not allow resolution of such coastal effects [*Bakun*, 1973; *Pickett and Schwing*, 2006]. Elsewhere, τ_b is weaker than τ_g, which is understood to be due to coastal drag, observed at the buoys but not captured by τ_g given its resolution.

[45] The broad minimum around N14 and N13 in both wind data sets is explained by a similar phenomenon, but operating at a larger scale. This is due to Cape Mendocino, which represents a large-scale change in coastal orientation [*Tjernström and Grisogono*, 2000; *Dorman et al.*, 2000], and the resulting downstream wind acceleration is large enough to be captured by the τ_g. The minimum in τ_b at N13 is then the result of the combined effect of accelerations due to Cape Mendocino and Point Arena, one nested within the other [*Edwards et al.*, 2002].

[46] Latitudinal differences in SST are caused by a combination of latitudinal trends in surface heating, strength of τ, and topography. While the τ minimum at N13 is accompanied by a SST minimum, this is not true at N28 (see Figures 2 and 6) in spite of similar topography and local hydraulic acceleration of wind. In contrast, N13 is located in a larger area of accelerated winds due to the large-scale effect of the bend in the coast at Cape Mendocino. This results in an increase of coastal upwelling and a region of strong positive wind stress curl that extends 200–300km from the shore and causes a broad shoaling of isotherms that further enhance coastal upwelling [*Bakun and Nelson*, 1991; *Enriquezand Friehe*, 1995; *Murphree et al.*, 2003]. In contrast, at N28 no large-scale acceleration of the wind (no τ_g minimum) is observed. Therefore, wind stress curl here is weak [*Bakun and Nelson*, 1991] or negative [*Beardsley et al.*, 1987], which combined with stronger surface heating at lower latitudes and seasonal heat transport from the south, results in coastal upwelling of shallower/warmer water than at N13 [*Lentz and Chapman*, 2004]. At N14, there is a minimum of τ_g, but local conditions determined by topography leads to slightly weaker upwelling forcing (τ_b) than at N13 and therefore, SST is not as low.

[47] Alongshore flow also varies with latitude, partly in association with the strength of the wind, but also due to the effect of topographic features. Preliminary results from prior hydrography and mooring studies [*Kosro*, 1987; *Largier et al.*, 1993] and regional HF-radar monitoring [*Kaplan and Lekien*, 2007; *Bjorkestedt et al.*, 2010; *Kim et al.*, 2011] indicate the presence of semi-permanent eddies and plumes during the upwelling and relaxation seasons. Further, it is well known that retention is associated with embayments between headlands and that this is seen as areas with high SST and Chl, characteristic of aged upwelled waters [*Largier et al.*, 1993; *Graham and Largier*, 1997; *Penven et al.*, 2002; *Largier*, 2004; *Kaplan and Largier*, 2006; *Vander Woude et al.*, 2006; *Oliveira et al.*, 2009; *Bjorkstedt et al.*, 2010]. On the other hand, cold-water, low-chlorophyll plumes stream south and offshore from upwelling centers, e.g., Point Mendocino, Point Arena and Point Sur, where wind stress and upwelling are strong [*Shannon*, 1985; *Strub et al.*, 1991; *Rosenfeld et al.*, 1994; *Halle and Largier*, 2011]. The most prominent embayment feature is observed in the Gulf of Farallones (Figure 9), demarcated by the chlorophyll minima near the headlands at Point Arena and Point Sur. While high Chl values are observed around buoy N13 (in spite of the strength of local winds), it is interesting to note that Chl peaks here in October following the seasonal demise of upwelling winds and enhanced northward transport of the high-chlorophyll waters from the Gulf of

Farallones past Point Reyes [*Strub et al.*, 1987; *Kaplan and Largier*, 2006; *Bjorkstedt et al.*, 2010]. In northern California, the area between Cape Blanco and Cape Mendocino also acts as a weakly retentive embayment, with weaker-than-elsewhere offshore transport in summer and fall [*Largier et al.*, 1993; *Bjorkestedt et al.*, 2010] allowing higher concentrations of phytoplankton to develop. A third, smaller retentive embayment is found in Monterey Bay (N42) [*Graham and Largier*, 1997], however, the highest Chl values are found closer to the shore than the buoy [see, e.g., *Graham and Largier*, 1997] and they are not captured by the satellite data transect chosen here.

5.3. Anomalies

[48] In California, variance in τ and SST at timescales longer than 3 months is split roughly evenly between intra-annual variability (3–12 months), annual variability (seasonal), and inter-annual variability (longer than 12 months), which differs from other upwelling regions where variance is dominated by inter- or intra-annual frequencies [*Chavez and Messié*, 2009]. Intra-annual anomalies represent strong persistent upwelling events in some years and a persistent absence of upwelling events in other years. In the north, however, there is more evidence for oceanic influences on intra-annual coastal variability, reflected in the increasing influence of PDO on SST and τ_b. In general, intra-annual SST is better correlated with τ_b than τ_g, indicating that in this timescale, variability is related to the coastal upwelling process.

[49] Inter-annual variability is well related to climate indices: to the basin-wide state of the north Pacific Ocean (PDO and NPGO), and to propagating perturbations in temperatures from the equatorial Pacific (ENSO/MEI). Although the cause of some of inter-annual and decadal anomalies are not fully understood [*Mantua and Hare*, 2002; *Di Lorenzo et al.*, 2010], large events of ENSO and PDO have been related to anomalies in coastal regions, particularly in SST [*Lluch-Cota et al.*, 2001; *Schwing et al.*, 2002; *Legaard and Thomas*, 2006], and to anomalies in biological productivity [e.g., *Thomas et al.*, 2009] and marine populations [*Cloern et al.*, 2010; *Black et al.*, 2011]. Since these are mainly large-scale oceanographic indices, they track and correlate better with SST anomalies than with local wind stress. τ_g however is well correlated with MEI in the center of the region and with PDO in the northern region, which is expected since the ultimate source of τ is related to the NE Pacific temperatures through the atmospheric pressure fields. At the coast however, this influence is combined with local changes in the ocean/atmospheric conditions, changing the correlation of these indices with τ_b. Inter-annual SST anomalies at the buoys are then a combination of large-scale influences from offshore (NE Pacific) and the effect of coastal upwelling winds. Furthermore, changes in coastal upwelling have also been related to a secular increase in global temperatures [*Bakun*, 1990]. Specifically, in central California, *García-Reyes and Largier* [2010] have reported a trend of stronger upwelling winds and colder SST at the NOAA buoys during the upwelling season and earlier spring transition from 1982 to 2008. Time series of the upwelling index, and large scale winds, since 1946 show similar trend of stronger upwelling in central California [*Bakun*, 1973; *Mendelssohn and Schwing*, 2002; *Black et al.*, 2011].

[50] Although many of the anomalies (Figure 11) can be related to climate events, some important anomalies are not related to any of the climate indices analyzed, like the anomalies in 1985 or the delayed upwelling season in 2005. The 2005 anomaly, which was only present in the north for τ_b but in all California for SST, has been related to an anomalous position of the jet stream [*Sydeman et al.*, 2006], a phenomena not tracked by any of the indices, leading to an anomaly in the time of the spring transition. This anomaly has also been linked to large anomalies in the ecosystem [*Mackas et al.*, 2006; *Schwing et al.*, 2006; *Sydeman et al.*, 2006].

[51] Anomalies in chlorophyll are difficult to relate to those in τ since Chl does not vary linearly with upwelling (Figure 10). However, years with large anomalies in τ_b lead to low Chl values, in agreement with an optimal window of productivity reported in other studies [*Cury and Roy*, 1989; *Gargett*, 1997; *Botsford et al.*, 2003]. Strong upwelling leads to rapid offshore transport and poor light conditions due to turbidity, while poor upwelling does not bring enough nutrients to the euphotic zone to fuel phytoplankton blooms, but moderate (and interrupted) upwelling winds allow nutrients to be upwelled and remain nearshore long enough time for phytoplankton population to grow [*Botsford et al.*, 2003, 2006]. SST anomalies also have an impact on Chl, since they are also seen in the stratification of the water column [*Palacios et al.*, 2004], affecting the source of upwelled water and its nutrient content, leading to anomalies in Chl or shifting the dominant phytoplankton species [*Estrada and Blasco*, 1979; *Murphree et al.*, 2003; *Lentz and Chapman*, 2004; *Kudela et al.*, 2005]. Further variability in Chl values could be related to changes in nutrient composition due to river runoff [*Kudela et al.*, 2008], presence of suspended particulates that affect satellite data, anomalous currents and advection of nutrients and phytoplankton, or changes in the frequency and length of upwelling and relaxation events [*Cury and Roy*, 1989; *Gargett*, 1997; *Botsford et al.*, 2003, 2006].

6. Conclusion

[52] The seasonality of coastal upwelling off central and northern California is clearly defined by an analysis of 29 years of buoy wind and SST data over the shelf. The Upwelling Season is defined as April-June, followed by a Relaxation Season characterized by weaker and less variable upwelling winds and warmer surface waters. During the Storm Season, winds are dominated by the passage of mid-latitude cold fronts.

[53] In the seasonality of upwelling and its anomalies, one sees the interplay of three factors in conditions over the shelf: coastal winds, large-scale winds, and offshore and remote ocean conditions. While the large scale winds that lead to positive wind stress curl act to lift isotherms over a region extending well beyond the shelf, the nearshore winds bend isotherms further upward and the coldest waters break the surface over the shelf. Ocean conditions, in particular surface temperature, affect large-scale and local winds, as well as affecting how the ocean responds to them. The strength of upwelling and the depth from which waters are upwelled are determined not only by the strength of local wind-forcing but also by the strength and depth of the

thermocline, which is related to the large-scale thermocline in the California Current and the North Pacific.

[54] In parallel, seasonal alongshore flow and primary productivity are also controlled by local winds, large-scale winds and ocean conditions. Thus by clarifying the seasonal structure in upwelling (winds and temperature) and the primary factors influencing this seasonality we build a foundation for an improved understanding of seasonal variability in marine population processes and more careful use of environmental indices in identifying primary environment-population links. Given the high productivity in upwelling systems, there is a compelling need to understand bottom-up influences on population levels at higher trophic levels - populations comprised of individuals that live for longer than a year and in which abundance and condition can be expected to depend on benefits or losses accrued due to the strength or timing of upwelling in preceding seasons.

[55] **Acknowledgments.** We thank R. Suryan from Oregon State University for compiling and providing the chlorophyll data, M. Losekoot from BML/UCDavis for compiling surface flow data, and W. Sydeman from the Farallon Institute for insight and encouragement in conducting these analyses. We also thank the anonymous reviewers whose comments greatly improved this manuscript.

References

Bakun, A. (1973), Coastal upwelling indices, West Coast of North America, 1946–71, *NOAA Tech. Rep. NMFS SSRF-671*, Natl. Oceanic and Atmos. Admin., Silver Spring, Md.

Bakun, A. (1990), Global climate change and intensification of coastal ocean upwelling, *Science*, *247*, 198–201.

Bakun, A., and C. S. Nelson (1991), The seasonal cycle of wind-stress curl in subtropical eastern boundary current regions, *J. Phys. Oceanogr.*, *21*, 1815–1834.

Barth, J. A., et al. (2007), Delayed upwelling alters nearshore coastal ocean ecosystems in the northern California Current, *Proc. Natl. Acad. Sci. U. S. A.*, *104*(10), 3719–3724.

Beardsley, R. C., et al. (1987), Local atmospheric forcing during the Coastal Ocean Dynamics Experiment: 1. A description of the marine boundary layer and atmospheric conditions over a Northern California upwelling region, *J.Geophys. Res.*, *92*(C2), 1467–1488.

Bjorkstedt, E. P., et al. (2010), State of the California Current 2009–2010: Regional variation persists through transition from La Niña to El Niño (and back?), *CalCOFI Rep. 51*, Calif. Coop. Oceanic Fish. Invest., San Diego, Calif.

Black, B. A., et al. (2011), Winter and summer upwelling modes and their biological importance in the California Current ecosystem, *Global Change Biol.*, *17*, 2536–2545, doi:101111/j.1365-2486.2011.024222.x.

Bograd, S., et al. (2002), On the changing seasonality over the North Pacific, *Geophys. Res. Lett.*, *29*(9), 1333, doi:10.1029/2001GL013790.

Bograd, S. J., et al. (2009), Phenology of coastal upwelling in the California Current, *Geophys. Res. Lett.*, *36*, L01602, doi:10.1029/2008GL035933.

Bond, N. A., C. F. Mass, and J. E. Overland (1996), Coastally trapped wind reversals along the United States West Coast during the warm season. Part I: Climatology and temporal evolution, *Mon. Weather Rev.*, *124*, 430–445.

Botsford, L. W., et al. (2003), Wind strength and biological productivity in upwelling systems: An idealized study, *Fish. Oceanogr.*, *12*(4/5), 245–259.

Botsford, L. W., et al. (2006), Effects of variable winds on biological productivity on continental shelves in coastal upwelling systems, *Deep Sea Res., Part II*, *53*, 3116–3140, doi:10.1016/j.dsr2.2006.07.011.

Burk, S. D., and W. T. Thompson (1995), The summertime low-level jet and marine boundary layer structure along the California coast, *Mon. Weather Rev.*, *124*, 668–686.

Chavez, F. P., and M. Messié (2009), A comparison of eastern boundary upwelling ecosystems, *Prog. Oceanogr.*, *83*, 80–96.

Chhak, K., and E. Di Lorenzo (2007), Decadal variations in the California Current upwelling cells, *Geophys. Res. Lett.*, *34*, L14604, doi:10.1029/2007GL030203.

Cloern, J. E., et al. (2010), Biological communities in San Francisco Bay track large-scale climate forcing over the North Pacific, *Geophys. Res. Lett.*, *37*, L21602, doi:10.1029/2010GL044774.

Cury, P., and C. Roy (1989), Optimal environmental window and pelagic fish recruitment success in upwelling areas, *Can. J. Fish. Aquat. Sci.*, *46*(4), 670–680.

Dever, E. P., and S. J. Lentz (1994), Heat and salt balances over the northern California shelf in winter and spring, *J. Geophys. Res.*, *99*(C8), 16,001–16,017.

Di Lorenzo, E., et al. (2008), North Pacific Gyre Oscillation links ocean climate and ecosystem change, *Geophys. Res. Lett.*, *35*, L08607, doi:10.1029/2007GL032838.

Di Lorenzo, E., et al. (2009), Nutrient and salinity decadal variations in the central and eastern North Pacific, *Geophys. Res. Lett.*, *36*, L14601, doi:10.1029/2009GL038261.

Di Lorenzo, E., et al. (2010), Central Pacific El Niño and decadal climate change in the North Pacific Ocean, *Nat. Geosci.*, *3*, 762–765, doi:10.1038/ngeo984.

Dorman, C. E., and C. D. Winant (1995), Buoy observations of the atmosphere along the west coast of the United States, 1981–1990, *J. Geophys. Res.*, *100*(C8), 16,029–16,044.

Dorman, C. E., et al. (2000), Large-scale structure of the June–July 1996 marine boundary layer along California and Oregon, *Mon. Weather Rev.*, *128*, 1632–1652.

Edwards, K. A., D. P. Rogers, and C. E. Dorman (2002), Adjustment of the marine atmospheric boundary layer to the large-scale bend in the California coast, *J. Geophys. Res.*, *107*(C12), 3213, doi:10.1029/2001JC000807.

Enriquez, A. G., and C. A. Friehe (1995), Effects of wind stress and wind stress curl variability on coastal upwelling, *J. Phys. Oceanogr.*, *25*, 1651–1671.

Estrada, M., and D. Blasco (1979), Two phases of the phytoplankton community in the Baja California upwelling, *Limnol. Oceanogr.*, *24*(6), 1065–1080.

García-Reyes, M., and J. Largier (2010), Observations of increased wind-driven coastal upwelling off central California, *J. Geophys. Res.*, *115*, C04011, doi:10.1029/2009JC005576.

Gargett, A. E. (1997), The optimal stability 'window': A mechanism underlying decadal fluctuations in North Pacific salmon stocks?, *Fish. Oceanogr.*, *6*(2), 109–117.

Graham, W. M., and J. L. Largier (1997), Upwelling shadows as nearshore retention sites: The example of northern Monterey Bay, *Cont. Shelf Res.*, *17*(5), 509–532.

Halle, C. M., and J. L. Largier (2011), Surface circulation downstream of the Point Arena upwelling center, *Cont. Shelf Res.*, *31*, 1260–1272, doi:10.1016/j.csr.2011.04.007.

Halliwell, G. R., Jr., and J. S. Allen (1987), The large-scale coastal wind field along the West Coast of North America, 1981–1982, *J. Geophys. Res.*, *92*(C2), 1861–1884.

Huyer, A. (1983), Coastal upwelling in the California Current System, *Prog. Oceanogr.*, *12*, 259–284.

Kahru, M., et al. (2009), Trends in primary production in the California Current detected with satellite data, *J. Geophys. Res.*, *114*, C02004, doi:10.1029/2008JC004979.

Kaplan, D. M., and J. Largier (2006), HF radar-derived origin and destination of surface waters off Bodega Bay, California, *Deep Sea Res., Part II*, *53*, 2906–2930, doi:10.1016/j.dsr2.2006.07.012.

Kaplan, D. M., and F. Lekien (2007), Spatial interpolation and filtering of surface current data based on open-boundary modal analysis, *J. Geophys. Res.*, *112*, C12007, doi:10.1029/2006JC003984.

Kaplan, D. M., J. Largier, and L. W. Botsford (2005), HF radar observations of surface circulation off Bodega Bay (northern California, USA), *J. Geophys. Res.*, *110*, C10020, doi:10.1029/2005JC002959.

Kaplan, D. M., J. D. Paduan, and J. Largier (2007), Analysis of coastal circulation in the California Current System from a large array of HF radars along the coast of northern California, paper presented at 54th Eastern Pacific Ocean Conference, Oreg. State Univ., Leavenworth, Wash.

Kim, S. Y., et al. (2011), Mapping the U.S. West Coast surface circulation: A multiyear analysis of high-frequency radar observation, *J. Geophys. Res.*, *116*, C03011, doi:10.1029/2010JC006669.

Koračin, D., et al. (2004), Perturbations of marine-layer winds, wind stress, and wind stress curl along California and Baja California in June 1999, *J. Phys. Oceanogr.*, *34*, 1152–1173.

Kosro, P. M. (1987), Structure of the coastal current field off Northern California during the Coastal Ocean Dynamics Experiment, *J. Geophys. Res.*, *92*(C2), 1637–1654.

Kudela, R., et al. (2005), Harmful algal blooms in coastal upwelling systems, *Oceanography*, *18*(2), 184–197.

Kudela, R., et al. (2008), New insights into the controls and mechanisms of plankton productivity in coastal upwelling waters in the Northern California Current Systems, *Oceanography*, *21*(4), 46–59.

Large, W. G., and S. Pond (1981), Open ocean momentum flux measurements in moderate to strong winds, *J. Phys. Oceanogr.*, *11*, 324–336.

Largier, J. L. (2003), Considerations in estimating larval dispersal distances from oceanographic data, *Ecol. Appl.*, *13*(1), S71–S89.
Largier, J. (2004), The importance of retention zones in the dispersal of larvae, *Am. Fish. Soc. Symp.*, *42*, 105–122.
Largier, J. L., B. A. Mangell, and C. D. Winant (1993), Subtidal circulation over the Northern California Shelf, *J. Geophys. Res.*, *98*(C10), 18,147–18,179.
Legaard, K. R., and A. C. Thomas (2006), Spatial patterns in seasonal and interannual variability of chlorophyll and sea surface temperature in the California Current, *J. Geophys. Res.*, *111*, C06032, doi:10.1029/2005JC003282.
Lentz, S. J. (1987), A description of the 1981 and 1982 spring transitions over the Northern California Shelf, *J. Geophys. Res.*, *92*(C2), 1545–1567.
Lentz, S. J., and D. C. Chapman (2004), The importance of nonlinear cross-shelf momentum flux during wind-driven coastal upwelling, *J. Phys. Oceanogr.*, *34*, 2444–2457.
Lluch-Cota, D. B., W. S. Wooster, and S. R. Hare (2001), Sea surface temperature variability in coastal areas of the northeastern Pacific related to the El Niño-Southern Oscillation and the Pacific Decadal Oscillation, *Geophys. Res. Lett.*, *28*(10), 2029–2032.
Lynn, R. J., et al. (2003), Seasonal renewal of the California Current: The spring transition off California, *J. Geophys. Res.*, *108*(C8), 3279, doi:10.1029/2003JC001787.
Mackas, D. L., et al. (2006), Zooplankton anomalies in the California Current system before and during the warm ocean conditions of 2005, *Geophys. Res. Lett.*, *33*, L22S07, doi:10.1029/2006GL027930.
Mantua, N., and S. R. Hare (2002), The Pacific Decadal Oscillation, *J. Oceanogr.*, *58*, 35–44.
Mendelssohn, R., and F. B. Schwing (2002), Common and uncommon trends in SST and wind stress in the California and Peru-Chile current systems, *Progr. Oceanogr.*, *53*, 141–162.
Mendelssohn, R., F. B. Schwing, and S. J. Bograd (2003), Spatial structure of the subsurface temperature variability in the California Current, 1950–1993, *J. Geophys. Res.*, *108*(C3), 3093, doi:10.1029/2002JC001568.
Murphree, T., et al. (2003), The seasonal cycle of wind stress curl and its relationship to subsurface ocean temperature in the northeast Pacific, *Geophys. Res. Lett.*, *30*(9), 1469, doi:10.1029/2002GL016366.
Nuss, W. A., et al. (2000), Coastally trapped wind reversals: Progress toward understanding, *Bull. Am. Meteorol. Soc.*, *81*(4), 719–743.
Nykjær, L., and L. Van Camp (1994), Seasonal and interannual variability of coastal upwelling along northwest Africa and Portugal from 1981 to 1991, *J. Geophys. Res.*, *99*(C7), 14,197–14,207.
Oliveira, P. B., et al. (2009), Surface temperature, chlorophyll and advection patterns during a summer upwelling event off central Portugal, *Cont. Shelf Res.*, *29*, 759–774, doi:10.1016/j.csr.2008.08.004.
Palacios, D. M., et al. (2004), Long-term and seasonal trends in stratification in the California Current, 1950–1993, *J. Geophys. Res.*, *109*, C10016, doi:10.1029/2004JC002380.
Penven, P., et al. (2002), Simulation of a coastal jet retention process using a barotropic model, *Oceanol. Acta*, *23*(5), 615–634.
Pickett, M. H., and F. B. Schwing (2006), Evaluating upwelling estimates off the west coast of North and South America, *Fish. Oceanogr.*, *15*(3), 256–269.
Rahn, D. A., R. D. Garreaud, and J. A. Rutllant (2011), The low-level atmospheric circulation near Tongoy Bay–Point Lengua de Vaca (Chilean coast, 30°S), *Mon. Weather Rev.*, *139*, 3638–3647, doi:10.1175/MWR-D-11-00059.1.
Rosenfeld, L. K., et al. (1994), Bifurcated flow from an upwelling center: A cold water source for Monterey Bay, *Cont. Shelf Res.*, *14*(9), 931–964.
Schroeder, I. D., et al. (2009), Winter pre-conditioning of seabird phenology in the California Current, *Mar. Ecol. Prog. Ser.*, *393*, 211–223, doi:10.3354/meps08103.
Schwing, F. B., et al. (2002), The evolution of oceanic and atmospheric anomalies in the northeast Pacific during the El Niño and La Niña events of 1995–2001, *Prog. Oceanogr.*, *54*, 459–491.
Schwing, F. B., et al. (2006), Delayed coastal upwelling along the U.S. West Coast in 2005: A historical perspective, *Geophys. Res. Lett.*, *33*, L22S01, doi:10.1029/2006GL026911.
Send, U., R. C. Beardsely, and C. D. Winant (1987), Relaxation from upwelling in the Coastal Ocean Dynamics Experiment, *J. Geophys. Res.*, *92*(C2), 1683–1698.
Shanks, A. L., and G. C. Roegner (2007), Recruitment limitation in Dungeness Crab populations is driven by variation in atmospheric forcing, *Ecology*, *88*(7), 1726–1737.
Shannon, L. V. (1985), The Benguela ecosystem: 1. Evolution of the Benguela, physical features and processes, *Oceanogr. Mar. Biol. Ann. Rev.*, *23*, 105–182.
Steger, J. M., et al. (2000), The circulation and water masses in the Gulf of the Farallones, *Deep Sea Res., Part II*, *47*, 907–946.
Ström, L., and M. Tjernström (2004), Variability in the summertime coastal marine atmospheric boundary-layer off California, USA, *Q. J. R. Meteorol. Soc.*, *130*, 423–448, doi:10.1256/q j.03.12.
Strub, P. T., et al. (1987), Seasonal cycle of currents, temperatures, winds, and sea level over the northeast Pacific continental shelf: 35N to 48N, *J. Geophys. Res.*, *92*(C2), 1467–1488.
Strub, P. T., M. Kosro, and A. Huyer (1991), The nature of the cold filaments in the California Current System, *J. Geophys. Res.*, *96*(C8), 14,743–14,768.
Sydeman, W. J., and S. J. Bograd (2009), Marine ecosystems, climate and phenology: Introduction, *Mar. Ecol. Prog. Ser.*, *39*, 185–301, doi:10.3354/meps08382.
Sydeman, W. J., et al. (2006), Planktivorous auklet *Ptychoramphys aleuticus* responses to ocean climate, 2005: Unusual atmospheric blocking?, *Geophys. Res. Lett.*, *33*, L22S09, doi:10.1029/2006GL026736.
Thomas, A. C., P. Brickely, and R. Weatherbee (2009), Interannual variability in chlorophyll concentrations in the Humboldt and California Current Systems, *Prog. Oceanogr.*, *83*, 386–392, doi:10.1016/j.pocean.2009.07.020.
Tjernström, M., and B. Grisogono (2000), Simulation of supercritical flow around points and capes in a coastal atmosphere, *J. Atmos. Sci.*, *57*, 108–135.
Vander Woude, A. J., J. L. Largier, and R. M. Kudela (2006), Nearshore retention of upwelled waters north and south of Point Reyes (northern California), *Deep Sea Res., Part II.*, *53*, 2985–2998, doi:10.1016/j.dsr2.2006.01.003.
Wilkerson, F. P., et al. (2006), The phytoplankton bloom response to wind events and upwelled nutrients during the CoOP West study, *Deep Sea Res., Part II.*, *53*, 3023–3048, doi:10.1016/j.dsr2.2006.07.007.
Winant, C. D., R. C. Beardsley, and R. E. Davis (1987), Moored wind, temperature, and current observations made during Coastal Ocean Dynamics Experiments 1 and 2 over the Northern California Continental Shelf and Upper Slope, *J. Geophys. Res.*, *92*(C2), 1569–1604.
Winant, C. D., et al. (1988), The marine layer off Northern California: An example of supercritical channel flow, *J. Atmos. Sci.*, *45*(23), 3588–3605.

M. García-Reyes and J. L. Largier, Bodega Marine Laboratory, University of California, Davis, Bodega Bay, CA 94923, USA. (solgarcia@ucdavis.edu; jlargier@ucdavis.edu)